EURASIP Journal on Applied Signal Processing 2005:3, 369–381

Jitter-Robust Orthogonal Hermite Pulses for Ultra-Wideband Impulse Radio Communications

Giuseppe Thadeu Freitas de Abreu
Centre for Wireless Communications, University of Oulu, Tutkijantie 2E, 90570 Oulu, Finland
Email: giuseppe@ee.oulu.fi

Craig John Mitchell
Division of Physics, Electrical and Computer Engineering, Graduate School of Engineering, Yokohama National University, 79-5 Hodogaya, Yokohama 240-8501, Japan
Email: craig@kohnolab.dnj.ynu.ac.jp

Ryuji Kohno
Division of Physics, Electrical and Computer Engineering, Graduate School of Engineering, Yokohama National University, 79-5 Hodogaya, Yokohama 240-8501, Japan
Email: kohno@kohnolab.dnj.ynu.ac.jp

Received 3 October 2003; Revised 23 April 2004

The design of a class of jitter-robust, Hermite polynomial-based, orthogonal pulses for ultra-wideband impulse radio (UWB-IR) communications systems is presented. A unified and exact closed-form expression of the auto- and cross-correlation functions of Hermite pulses is provided. Under the assumption that jitter values are sufficiently smaller than pulse widths, this formula is used to decompose jitter-shifted pulses over an orthonormal basis of the Hermite space. For any given jitter probability density function (pdf), the decomposition yields an equivalent distribution of N-by-N matrices which simplifies the convolutional jitter channel model onto a multiplicative matrix model. The design of jitter-robust orthogonal pulses is then transformed into a generalized eigendecomposition problem whose solution is obtained with a Jacobi-like simultaneous diagonalization algorithm applied over a subset of samples of the channel matrix distribution. Examples of the waveforms obtained with the proposed design and their improved auto- and cross-correlation functions are given. Simulation results are presented, which demonstrate the superior performance of a pulse-shape modulated (PSM-) UWB-IR system using the proposed pulses, over the same system using conventional orthogonal Hermite pulses, in jitter channels with additive white Gaussian noise (AWGN).

Keywords and phrases: ultra-wideband communications, impulse radio, Hermite pulses, orthogonal design, jitter robustness, pulse-shape modulation.

1. INTRODUCTION

Hermite polynomial-based orthogonal pulses—also known as *Hermite pulses* or simply *Hermites*—were proposed in [1] for pulse-shape modulated (PSM-) ultra-wideband impulse radio (UWB-IR) communications, as an alternative to the pulse-position modulated (PPM) scheme first presented in [2]. Later, it was also shown that PSM and PPM can be combined into a pulse-shape and pulse-position modulation (PSPM) scheme [3].

A number of alternative orthogonal pulse-shape designs for UWB-IR communications based on different elementary functions have also been considered [4, 5, 6]. These works have, however, contributed to demonstrating the advantages of Hermite pulses which are smooth functions (differentiable in $\mathbb{R}$), well concentrated in both time and frequency domains, and easily derived through successive derivation and scaling of the Gaussian pulse [1].

Unfortunately, some properties of higher-order Hermites deteriorate faster, compared to those of lower-order ones. For instance, higher-order Hermites exhibit autocorrelation functions with narrower main-lobes and cross-correlation functions with more side-lobes than their lower-order counterparts. In addition, the spectra of higher-order Hermite pulses are less smooth and are slightly shifted towards higher frequencies compared to those of lower-order Hermites.

The orthogonality and smoothness of Hermite pulses, however, can be exploited to design new Hermite polynomial-based waveforms that mitigate these problems. One example is the design given in [7], where conventional (or

elementary) Hermites are combined yielding finite sets of pulses with no DC components and similar spectra. Another is the technique presented in [8], where the fact that a finite set of N different normalized orthogonal Hermite pulses form an orthonormal basis of an N-dimensional Hermite space [9] used to design Hermite waveforms which mitigate the distortion caused by differentiating antennas.

Mutual orthogonality among several pulses, however, depends on the perfect synchronization of all coexisting waveforms even in a single-user scenario. This ideal condition is not found in practical UWB-IR channels due to small, random mismatches (jitter) between the moment a transmitted pulse reaches the receiver and the instant the bank of correlators is triggered to perform detection. End-to-end link root mean square (RMS) jitter of a few tens of picoseconds have been reported as typical in UWB-IR channels [10] and shown to significantly reduce the performance of UWB systems using the conventional monocycle waveform. Since the monocycle is in fact the Hermite pulse of lowest- (zeroth-) order, the degradation due to jitter is expected to be severer in systems using more (higher-order) Hermites. In this paper, the powerful Hermite-space approach used in [8] is again invoked in order to design jitter-robust waveforms for UWB-IR systems.

Orthogonal pulse shapes have a broader range of potential applications in UWB-IR systems than modulation schemes. For instance, it is known that pseudorandom hopping sequences can be designed to effectively eliminate spectral lines in the power spectral density (PSD) of a UWB-IR signal [11, 12, 13]. Orthogonal "shape-time" designs have therefore the potential to achieve the same results with sequences of much shorter lengths since these can be seen as portions of a long time-hopping sequences running in parallel.

Orthogonal pulses can also be used in synchronous systems to separate different users or channels sharing the same spectrum. A prospective vision employing this idea is that of electronic appliances with distributed architectures [14]. The performance of all these applications would be similarly susceptible to degradation due to jitter.

Having made this remark, the technique introduced in this paper is presented in the context of its application to PSM schemes in a single-user scenario, only so that the results can be compared against those of [1]. The rest of the paper is arranged as follows. In Section 2, the PSM scheme for UWB-IR communications is briefly described and analyzed. A few ideas underlining the criterion for jitter-robust design are also given in this section. The new multiplicative jitter channel model is introduced in Section 3 laying the ground for the introduction of the design technique itself in Section 4. The correlation properties of the waveforms obtained with the proposed design are analyzed in Section 5. In Section 6, simulation results of a PSM-UWB-IR system are given which illustrate the effectiveness of the proposed pulses in combating jitter. Conclusions are drawn in Section 7.

2. PSM-UWB-IR SYSTEMS IN NOISY JITTER CHANNELS

Let $n \in \{0, \ldots, N-1\}$ be the integer equivalent to a binary codeword of length $\log_2(N)$, where $N \in \mathbb{N}^+$ is a power of 2. An N-ary PSM-UWB-IR system [1] maps each binary codeword onto an orthogonal waveform $\lambda_n(t)$. In a UWB-IR system, the duration T_p of each transmit waveform (pulse) is typically much smaller then the interval between consecutive transmissions T_s, so that the bandwidth of the transmitted signal is very large [15]. In order to achieve high data rates, T_s is made very small, which implies that T_p must be even smaller. A typical value of T_p is 1 nanosecond, which (in theory) enables data rates from several hundreds of Mbps to a few Gbps.

Assuming a nondistortive, single-user channel and perfect synchronization, the received signal corresponding to the nth codeword is given by

$$r_n(t) = \alpha_n \lambda_n(t) + w(t), \tag{1}$$

where α_n is the path loss and the noise waveform $w(t)$ is a stationary random process with a Gaussian probability density function (pdf), zero mean, and variance σ_w^2, which may also model interference [15].

If all orthogonal pulses $\lambda_n(t)$ occupy approximately the same band, it is fair to assume that the path losses α_n are the same for all pulses. This is the case of Hermite pulses and consequently, α_n are hereafter normalized to unity.

When the nth pulse $\lambda_n(t)$ is transmitted, the mth correlator output is simply

$$\int_{-T_p/2}^{T_p/2} r_n(t)\lambda_m(t)dt = \delta_{n,m} + w_m, \tag{2}$$

where w_m is the projection of the real additive white Gaussian noise (AWGN) waveform $w(t)$ onto $\lambda_m(t)$ and $\delta_{n,m}$ is the Kronecker delta given by

$$\delta_{n,m} = \begin{cases} 0 & \text{if } n \neq m, \\ 1 & \text{if } n = m. \end{cases} \tag{3}$$

Without loss of generality, all $\lambda_n(t)$ are assumed to have unitary energy and to be centered at $t = 0$. If the correlators are noiseless and employ $\lambda_n(t)$ as templates, the randoms $\{w_0, \ldots, w_{N-1}\}$ are independent and identically distributed (i.i.d), with zero mean and variance σ_w^2/N [16]. The pdf of noise at the output of each correlator is then given by

$$p\left(w_n; 0, \frac{\sigma_w^2}{N}\right) = \frac{1}{\sigma_w}\sqrt{\frac{N}{2\pi}}e^{-Nw_n^2/2\sigma_w^2}. \tag{4}$$

In the presence of jitter, however, the templates $\lambda_n(t)$ are shifted by an amount τ relative to $r_n(t)$, so that the mth correlator outputs

$$\gamma_m = \int_{-T_p/2}^{T_p/2} r_n(t)\lambda_m(t-\tau)dt = R_{\lambda_{n,m}}(\tau) + w_m, \tag{5}$$

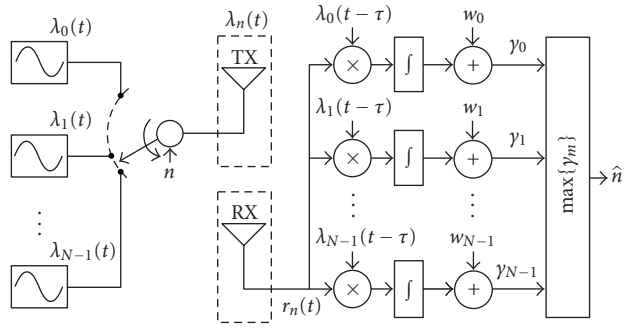

Figure 1: Structure of a simple PSM scheme for UWB-IR systems. Symbols are mapped onto set of orthonormal waveforms $\lambda_n(t)$. The receiver correlates the received signal with templates to all possible transmit waveforms. The variable τ indicates jitter disturbances. Detection is performed in a symbol-by-symbol maximum likelihood manner.

where $R_{\lambda_{n,m}}(\tau)$ is the cross-correlation function between the nth and the mth waveforms.

In the simplest, noncoherent case (when the receiver has no knowledge as to whether receive pulses are inverted or not), detection is carried out by selecting the correlator with the largest output magnitude. This process is mathematically described by

$$\hat{n} = \{k \mid |\gamma_k| > |\gamma_m(\tau)| \ \forall m\}. \tag{6}$$

The binary codeword corresponding to $\hat{n}$ is the symbol-by-symbol maximum likelihood estimate of the transmitted codeword. A schematic diagram of this PSM-UWB-IR system is shown in Figure 1.

In order to elaborate further, we assume that jitter is a real white Gaussian process with zero mean, variance σ_τ^2, and pdf given by

$$p(\tau; 0, \sigma_\tau^2) = \frac{1}{\sqrt{2\pi}\sigma_\tau} e^{-\tau^2/2\sigma_\tau^2}. \tag{7}$$

The pairwise probability $P_{n\to m}$, that an erroneous decision in favor of the mth symbol is made when the nth order pulse is received, is equal to the probability that the output of the mth correlator is larger than the output of the nth correlator. Given the noise and jitter processes characterized above, this can be expressed as

$$P_{n\to m} = \int_0^\infty p(|\gamma_m| > \Gamma) \cdot p(|\gamma_n| < \Gamma) d\Gamma, \tag{8}$$

where

$$\begin{aligned} p(|\gamma_n| < \Gamma) &= \int_{-\Gamma}^{\Gamma} p(\tau; R_{\lambda_{n,n}}(\tau), \sigma_\tau^2) d\tau, \\ p(|\gamma_m| > \Gamma) &= 1 - \int_{-\Gamma}^{\Gamma} p(\tau; R_{\lambda_{m,n}}(\tau), \sigma_\tau^2) d\tau. \end{aligned} \tag{9}$$

Taking the outputs of all correlators into account, the probability that the nth waveform is mistaken for any other waveform is simply

$$P_E(n) = \sum_{\substack{m=0 \\ m\neq n}}^{N-1} P_{n\to m}. \tag{10}$$

Finally, if P_n denotes the probability that the source outputs the nth codeword, the symbol error probability P_{E_S} is given by

$$P_{E_S} = \sum_{n=0}^{N-1} P_n P_E(n). \tag{11}$$

In most practical cases, all symbols in the transmit alphabet are equally likely, so that the averaged bit error probability P_{E_B} is related to the symbol error probability by [16]

$$P_{E_B} = \frac{N}{2(N-1)} P_{E_S}. \tag{12}$$

The PSM-UWB-IR system described here falls within the classic theory of correlation-based systems [16]. In principle, closed-form expressions of the probabilities given above can be derived with knowledge of the cross-correlation functions $R_{\lambda_{n,m}}(\tau)$, which depend on the shapes of $\lambda_n(t)$. In practical cases, however, the complexity of the functions $R_{\lambda_{n,m}}(\tau)$ can make the derivation of closed forms of $P_{n\to m}$ extremely difficult.

Equations (9) clearly indicate, however, that the presence of jitter causes the correlators to sample the functions $R_{\lambda_{n,m}}(\tau)$ not exactly at the origin, but at random points in its vicinity, altering the detection metrics γ_m and degrading the performance of the system. This suggests that robustness against jitter can be forged by designing waveforms that exhibit autocorrelations which remain as close to one as possible within a vicinity of the origin and cross-correlations which remain as close to zero as possible in that interval.

In the next section, the influence of jitter over the correlation properties of conventional Hermite pulses and its impact on the performance of PSM-UWB-IR schemes using Hermites is analyzed in further detail.

3. HERMITE PULSES IN THE JITTER CHANNEL

3.1. Hermite decomposition

Let the Hermite polynomial of order n be defined in the interval $(-\infty, \infty)$ by the Rodrigues formula [9]

$$H_n(t) \triangleq (-1)^n e^{t^2} \frac{d^n}{dt^n} e^{-t^2}, \quad n \in \mathbb{N}. \tag{13}$$

Orthogonal Hermite pulses [7] can then be defined as

$$\psi_n(t) \triangleq \mathcal{N}_n e^{-t^2/2} H_n(t), \tag{14}$$

where $\mathcal{N}_n$ is a factor that normalizes the energy of $\psi_n(t)$ to unity.

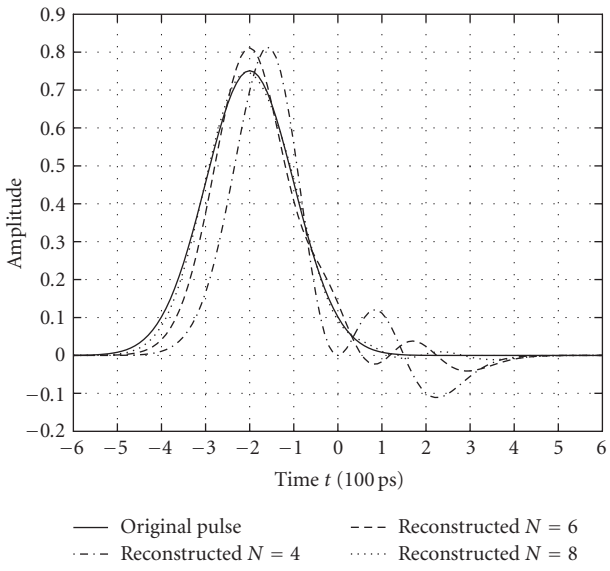

FIGURE 2: Reconstruction of a zeroth-order Hermite pulse shifted (e.g., due to jitter) by 200 picoseconds. Hermite spaces of larger dimensions yield more accurate recomposed waveforms than smaller ones.

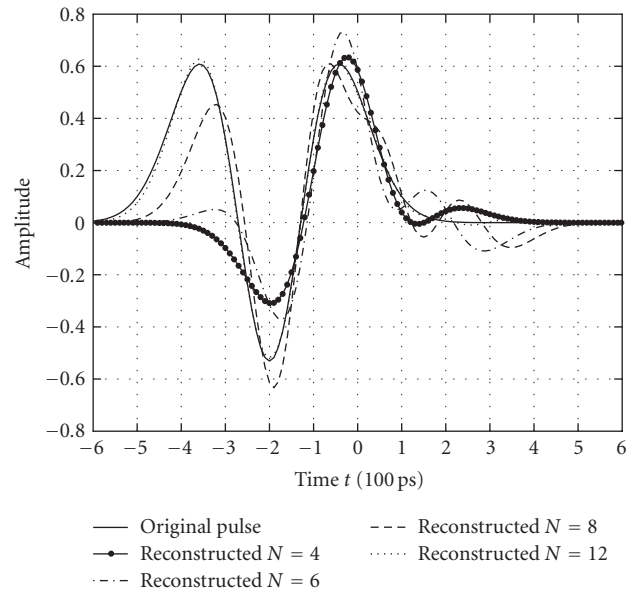

FIGURE 3: Reconstruction of a second-order Hermite pulse shifted (e.g., due to jitter) by 200 picoseconds. Higher-order Hermite pulses require Hermite spaces of larger dimensions in order to yield accurate recomposed waveforms.

Although an alternative definition of orthogonal Hermites was utilized in [1], we have shown in [17] that both definitions are equivalent in terms of their correlation properties.

The normalization coefficients $\mathcal{N}_n$ are directly obtained from the orthogonality property of Hermite polynomials [9]:

$$\int_{-\infty}^{\infty} e^{-t^2} H_n(t) H_m(t) dt = \delta_{n,m} 2^n n! \sqrt{\pi}. \tag{15}$$

This gives

$$\mathcal{N}_n = \frac{1}{\sqrt{2^n n! \sqrt{\pi}}}, \tag{16}$$

and consequently,

$$\int_{-\infty}^{\infty} \psi_n(t) \psi_m(t) dt = \delta_{n,m}. \tag{17}$$

Hermite pulses as defined in (14) are normalized, orthogonal, smooth functions of t and as such form an orthonormal basis $\mathbf{\Psi} = \{\psi_0(t), \psi_1(t), \dots\}$ of a Hermite space [9]. If jitter values are sufficiently smaller than the pulse widths, $\psi_n(t-\tau)$ can be represented as linear combinations of the elements of $\mathbf{\Psi}$, with coefficients given by

$$\psi_n(t-\tau) = \sum_{m=0}^{\infty} c_{m,n}(\tau) \psi_m(t). \tag{18}$$

Multiplying (18) by $\psi_m(t)$, integrating over the interval $(-\infty, \infty)$, and making use of the pulse orthogonality property given in (17), we have

$$c_{m,n}(\tau) = \int_{-\infty}^{\infty} \psi_m(t) \psi_n(t-\tau) dt = R_{\psi_{m,n}}(\tau). \tag{19}$$

In other words, the coefficients $c_{m,n}(\tau)$ are the cross-correlation functions $R_{\psi_{m,n}}(\tau)$ between the nth and the mth order pulses at the point τ. Through laborious combinations of standard results on the integration of Hermite polynomials [9], we have found the following unified closed-form expression for the auto- and cross-correlation functions $R_{\psi_{m,n}}(\tau)$:

$$R_{\psi_{m,n}}(\tau) = \begin{cases} \dfrac{(-1)^{2m+n} \tau^{n+m} \sqrt{n!m!}}{\sqrt{2^{n+m}}} e^{-\tau^2/4} & \\ \times \sum_{k=0}^{\min(n,m)} \dfrac{(-1)^k \tau^{-2k} \sqrt{4^k}}{(n-k)!(m-k)!k!} & \text{if } \tau \neq 0, \\ \delta_{m,n} & \text{if } \tau = 0. \end{cases} \tag{20}$$

In practice, there is a limit to the size of the Hermite space used, given by the number of waveform generators or correlators available. This results in a truncation of (18) and a tradeoff between decomposition accuracy and complexity. Figures 2 and 3, respectively, show zeroth- and second-order Hermite pulses, shifted by $\tau = 200$ picoseconds, reconstructed with the Hermite series given in (18) truncated at different values of N (Hermite spaces of different sizes). Generally, the larger the order of $\psi_n(t-\tau)$ and the amount τ by which it is shifted, the larger the size N of the Hermite space required for an accurate representation.

In the UWB-IR literature, the received waveforms corresponding to transmit UWB pulses are often assumed to be their second derivatives [2, 10, 11, 12, 17]. Although in theory this differentiating distortion can be compensated with integrating circuits, in practice, this approach is unreliable as it may amplify noise and interference. We have shown that indeed derivatives of orthogonal Hermite pulses are not orthogonal receive waveforms [17].

In this paper, however, differentiating distortion effects is not taken into consideration for the following reasons. Firstly, we have previously derived a Hermite space method to design Hermite pulses whose second derivatives are orthogonal waveforms [8]. That technique can be straightforwardly combined with the one presented in this paper.

Secondly, recent research indicates that the UWB-IR channel can act as an integrator [18], such that the combined effects of two differentiating antennas (transmit and receive) and the channel is a single, not double, differentiation. Again in this case, the method presented in [8] can be easily modified and combined with the jitter-robust design for adequate compensation.

Finally, research on UWB antennas [19, 20] have shown that antennas can also exhibit resistive or inductive behaviors, respectively, resulting in outputs proportional to the input or to its integral.

In other words, it cannot be said that the differential-distortion model always applies to UWB-IR antennas and, in the particular cases when it does, adequate adjustments provided in [8] can be straightforwardly incorporated.

3.2. Jitter channel model

In narrowband communications theory the jitter channel is often described by a unitary impulse response convolutional model [16]. In this model, a shifted waveform $\lambda(t-\tau)$ is represented by

$$\lambda(t-\tau) = \lambda(t) * \delta(t-\tau) = \int_{-\infty}^{\infty} \lambda(x)\delta(x-\tau)dx, \quad (21)$$

where $*$ denotes the convolution and $\delta(t)$ is the unitary impulse at $t = 0$.

Given the extremely short duration of UWB pulses, it is difficult to adequately apply signal processing techniques developed under such a model to UWB-IR systems. The Hermite decomposition discussed in Section 3.1 can, however, be used to construct a new, multiplicative jitter channel model for UWB-IR communications, offering interesting possibilities from the signal-processing point of view. Before we proceed, however, a few more words about the properties of the jitter process in correlation-based UWB-IR systems must be said.

Jitter processes are typically uncorrelated in the time domain [10] and may be independent at different correlators if it is considered that their circuits are independently built and require the generation of template waveforms of different complexities and shapes. We refer to such a model as the *independent* jitter model.

For design purposes, however, it proves convenient to assume that the same jitter process affects all correlators simultaneously, as if all circuits were sharply synchronized but triggered by a common jittery clock. This is hereafter referred to as the *coherent* jitter model. The term *coherent* refers to the correlation of jitter processes in the *pulse-shape domain* and must not be confused with time coherence!

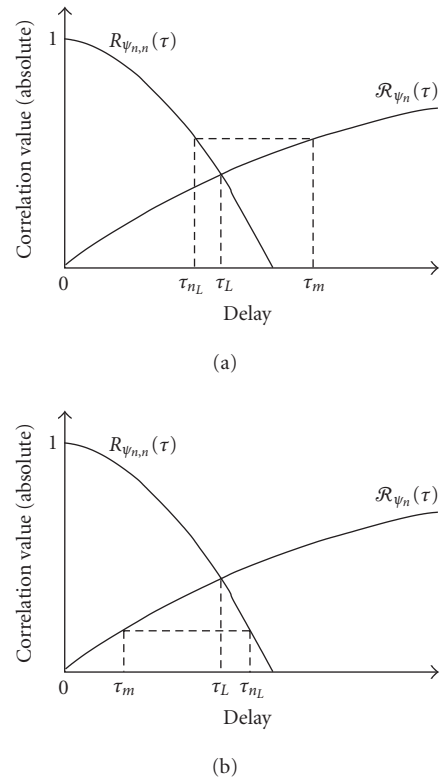

Figure 4: Typical relationship between critical jitter values τ_{n_L} and τ_L in an independent jitter channel. The magnitude of the gradient of the autocorrelation functions $R_{\psi_{n,n}}$ are typically larger than that of the envelope cross-correlation functions $\mathcal{R}_{\psi_n}$ in the vicinity of $\tau = 0$. Consequently, in average, $|\tau_{n_L}| > |\tau_m|$, which makes the independent jitter channel less severe than the coherent jitter channel. (a) Case 1: $|\tau_m| > |\tau_L|$. (b) Case 2: $|\tau_m| < |\tau_L|$.

In addition to enabling significant simplification in the jitter-robust design, the use of the coherent jitter model results in overdimensioning the jitter-robust waveforms and therefore does not compromise performance (Section 6). This is because coherent jitter is a worst-case scenario of the independent jitter channel, which can be shown as follows.

Let $\mathcal{R}_{\psi_n}(\tau)$ be the envelope of the cross-correlation functions $R_{\psi_{m,n}}(\tau)$:

$$\mathcal{R}_{\psi_n}(\tau) \triangleq \max\{R_{\psi_{0,n}}(\tau), \ldots, R_{\psi_{N-1,n}}(\tau)\}. \quad (22)$$

Typically, $|R_{\psi_{n,n}}(\tau)|$ decreases with $|\tau|$ in the vicinity of $\tau = 0$, while $|\mathcal{R}_{\psi_n}(\tau)|$ increases in the same interval. There is, therefore, a critical value τ_L such that (see Figure 4)

$$\tau_L \triangleq \left\{ \min\{|\tau|\} \;\middle|\; \begin{array}{l} (1)\; R_{\psi_{n,n}}(\tau) = \mathcal{R}_{\psi_n}(\tau), \\ (2)\; |R_{\psi_{n,n}}(\tau)| < |\mathcal{R}_{\psi_n}(\tau')| \quad \forall \tau' > \tau \end{array} \right\}. \quad (23)$$

In the absence of noise, the error probability $P_E(n)|_{\text{Coherent}}$ is simply the probability of having a jitter

value τ such that $|\tau| > |\tau_L|$. This gives

$$P_E(n)\big|_{\text{Coherent}} = 2\int_{\tau_L}^{\infty} p(\tau; 0, \sigma_\tau^2)\, d\tau. \tag{24}$$

In contrast, with an independent jitter channel, given an N-tuple of instantaneous jitter values $\vec{\tau} = \{\tau_0, \ldots, \tau_{N-1}\}$ affecting the receiver, $P_E(n)\big|_{\text{Noncoherent}}$ is determined by a dominant pair of correlators (m, n) such that $R_{\psi_{m,n}}(\tau_m) = \mathcal{R}_{\psi_n}(\tau_m)$ and the nth correlator is matched to the received pulse.

Since the jitter pdf and $R_{\psi_{m,n}}(\tau)$ are all symmetric functions, we hereafter simplify the notation by assuming τ to be positive, without loss of generality.

Let (τ_m, τ_n) be the jitter values observed at the dominant correlators and define the variable

$$\tau_{n_L} \triangleq \{\tau \mid R_{\psi_{n,n}}(\tau) = \mathcal{R}_{\psi_n}(\tau_m)\}. \tag{25}$$

Stating that an error will occur if $|R_{\psi_{m,n}}(\tau_m)| > |R_{\psi_{n,n}}(\tau_n)|$ is then equivalent to stating that $\tau_n > \tau_{n_L}$ (see Figure 4). The probability of error $P_E(n)\big|_{\text{Noncoherent}}$ then becomes

$$P_E(n)\big|_{\text{Noncoherent}} = 2\int_{\tau_{n_L}}^{\infty} p(\tau_n; 0, \sigma_\tau^2)\, d\tau_n. \tag{26}$$

The difficulty in using (26) lies in the need to find an expression for τ_{n_L}, which depends on both $R_{\psi_{n,n}}(\tau)$ and $\mathcal{R}_{\psi_n}(\tau)$. Handling the closed-form expression given in (20), however, we learn that for any given n, $R_{\psi_{n,n}}(\tau)$ exhibits a steeper slope in the vicinity of $\tau = 0$ than $\mathcal{R}_{\psi_n}(\tau)$. In other words, for a sufficiently small random τ_m, we have $|\tau_L - \tau_m| > |\tau_L - \tau_{n_L}|$ (see Figure 4), which can be written as $|\tau_L - \tau_m| = k|\tau_L - \tau_{n_L}|$ with $k > 1$. Thus

$$\tau_{n_L} = \frac{k+1}{k}\tau_L - \frac{\tau_m}{k}. \tag{27}$$

Equation (27) signifies that if τ_m is a zero-mean process with variance σ_τ^2, τ_{n_L} is a process with mean $((k+1)/k)\tau_L$ and variance σ_τ^2/k^2. Consequently, τ_{n_L} is in most cases larger than τ_m, which from (24) and (26) implies

$$P_E(n)\big|_{\text{Noncoherent}} < P_E(n)\big|_{\text{Coherent}}. \tag{28}$$

This shows that the coherent jitter model results in an overestimation of the impact of jitter and completes our argument.

Henceforth, the coherent jitter model is assumed unless stated otherwise.

The real N-by-N matrices $\mathbf{A}(\tau)$ which model the coherent jitter channel are given by

$$\mathbf{A}(\tau) = \begin{bmatrix} c_{0,0}(\tau) & c_{0,1}(\tau) & \cdots & c_{0,N-1}(\tau) \\ c_{1,0}(\tau) & c_{1,1}(\tau) & \cdots & c_{1,N-1}(\tau) \\ \vdots & \vdots & \ddots & \vdots \\ c_{N-1,0}(\tau) & c_{N-1,1}(\tau) & \cdots & c_{N-1,N-1}(\tau) \end{bmatrix}. \tag{29}$$

Let $\vec{\psi}_n$ denote the vector of coefficients $c_{m,n}$ of the N-truncated series representation of the nth-order transmit pulse $\psi_n(t)$. From (17) and (18), we have

$$\vec{\psi}_n \triangleq [c_{0,n}, \ldots, c_{N-1,n}]^{\mathrm{T}} = [\delta_{0,n}, \ldots, \delta_{N-1,n}]^{\mathrm{T}}. \tag{30}$$

Then, the vector representation of the corresponding noiseless receive waveform, in the presence of a jitter amount τ, is simply

$$\vec{\psi}_n\big|_\tau = \mathbf{A}(\tau)\vec{\psi}_n = \sum_{m=0}^{N-1} c_{m,n}(\tau)\vec{\psi}_m. \tag{31}$$

Note that despite the truncation at Nth term made in (31), the effect of jitter at the receiver is precisely described by the model since the entries of $\vec{\psi}_n\big|_\tau$ are the outputs of its bank of correlators, based on which detection is performed.

A number of alternative Hermite-based waveforms can be composed by combining several pulses $\psi_n(t)$ with adequate coefficients. We denote the vector representation of a waveform resulting from one such combination by $\vec{\phi}$. From the linearity of (31), it is clear that the vector representation of the corresponding receive waveform is given by

$$\vec{\phi}\big|_\tau = \mathbf{A}(\tau)\vec{\phi}. \tag{32}$$

In the next section, we show how such combined waveforms can be designed so as to yield jitter-robust Hermite pulses.

4. DESIGN OF JITTER-ROBUST ORTHOGONAL HERMITE PULSES

4.1. Design method

Equation (32) indicates that if a few vectors $\vec{\phi}_n$ can be properly designed such that

$$\begin{aligned} \vec{\phi}_n\big|_\tau &\approx \rho_n(\tau)\vec{\phi}_n, \\ \vec{\phi}_n \cdot \vec{\phi}_m &= \delta_{n,m}, \end{aligned} \tag{33}$$

the corresponding waveforms will be orthonormal pulses which retain orthogonality in the presence of jitter.

Equations (33) state a classic generalized eigenproblem over the infinite set of matrices $\mathbf{A}(\tau)$. In other words, the problem of designing jitter-robust Hermite waveforms is translated onto a simultaneous diagonalization problem. An approximate, numeric solution to this problem can be obtained as follows.

Define a finite set $\mathcal{A}_K = \{\mathbf{A}(\tau_0), \ldots, \mathbf{A}(\tau_{K-1})\}$ of matrices $\mathbf{A}(\tau_k)$, each corresponding to a different jitter value. The probability $p(|\tau_{k-1}| \le |\tau| < |\tau_k|)$ that an instantaneous jitter shift τ has magnitude between $|\tau_{k-1}|$ and $|\tau_k|$ ($|\tau_{k-1}| \le |\tau_k|$) is given by

$$p(|\tau_{k-1}| \le |\tau| < |\tau_k|) = 2\int_{\tau_{k-1}}^{\tau_k} \frac{1}{\sqrt{2\pi}\sigma_\tau} e^{-\tau^2/2\sigma_\tau^2}\, d\tau. \tag{34}$$

It is natural to fit the robustness of the waveforms to the probabilities of jitter occurrence. This can be accomplished by selecting the K jitter values τ_k such that

$$p(|\tau_0| \le |\tau| < |\tau_1|) = \cdots = p(|\tau_{K-1}| \le |\tau| < \infty). \tag{35}$$

Since each $\mathbf{A}(\tau_k)$ models a channel with delay τ_k, we refer to $\mathcal{A}_K$ as the set of *channel samples*. At this point, it becomes clear why, as suggested in Section 3.2, the use of a coherent jitter channel model significantly simplifies the design. Indeed, if an independent jitter model were assumed, the jitter pdf would be N-dimensional and a mesh of a significantly larger number of points would be necessary in order to sample the channel at equiprobable N-tuples $\vec{\tau}_k$ and construct the set of matrices $\mathbf{A}(\vec{\tau}_k)$ to be jointly diagonalized.

The set $\mathcal{A}_K$ can then be jointly diagonalized with the numerically robust, iterative algorithm proposed in [21]. This joint-diagonalization algorithm performs simultaneous similarity transformations over the whole set $\mathcal{A}_K$ by the successive application of Givens rotations. At each iteration, the angle of the Givens rotation is chosen so as to minimize a cost function which measures the distance of the set to the identity matrix (Jacobi angle). Details on the algorithm, as well as a thorough investigation on its properties, convergency and robustness to error perturbations are given in [21]. Fortunately, in [22], a closed-form expression of the optimal Jacobi angles used at each step in the joint-diagonalization algorithm [21] was provided, significantly reducing the computation complexity of the method.

The solution provided by [22] is the product of all similarity transformations, giving an orthonormal N-by-N matrix $\mathbf{X}$ such that

$$\mathbf{X} \in \mathbb{R}^{n\times n} \left| \begin{array}{l} (1)\ \mathbf{X}^{\mathrm{T}}\mathbf{X} = \mathbf{X}^{-1}\mathbf{X} = \mathbf{I}, \\ (2)\ \mathbf{X}^{\mathrm{T}}\mathbf{A}(\tau_k)\mathbf{X} \approx \mathbf{D}_k \quad \forall \tau_{k=0,1,\ldots,K-1}. \end{array} \right. \tag{36}$$

Comparing (33) to the solution (36), it is clear that the nth column $\vec{\chi}_n$ of $\mathbf{X}$ is the vector representation of a combination of Hermite pulses yielding a jitter-robust pulse. Mathematically, $\vec{\chi}_n$ are approximate eigenvectors to all matrices in $\mathcal{A}_K$ such that

$$\mathbf{A}(\tau_k)\vec{\chi}_n \approx \rho_n(\tau_k)\vec{\chi}_n, \tag{37a}$$

$$\vec{\chi}_n \cdot \vec{\chi}_m = \delta_{n,m}, \tag{37b}$$

where $\rho_n(\tau_k)$ is the eigenvalue associated with the generalized eigenvector $\vec{\chi}_n$ of the jitter matrix $\mathbf{A}(\tau_k)$.

Equations (37a) and (37b) are, respectively, equivalent to (33). The nth-order jitter-robust waveform $\phi_n(t)$ is simply the combination of elementary Hermite pulses using the entries of $\vec{\chi}_n$ as coefficients:

$$\phi_n(t) = \sum_{m=0}^{N-1} x_{m,n}\psi_m(t). \tag{38}$$

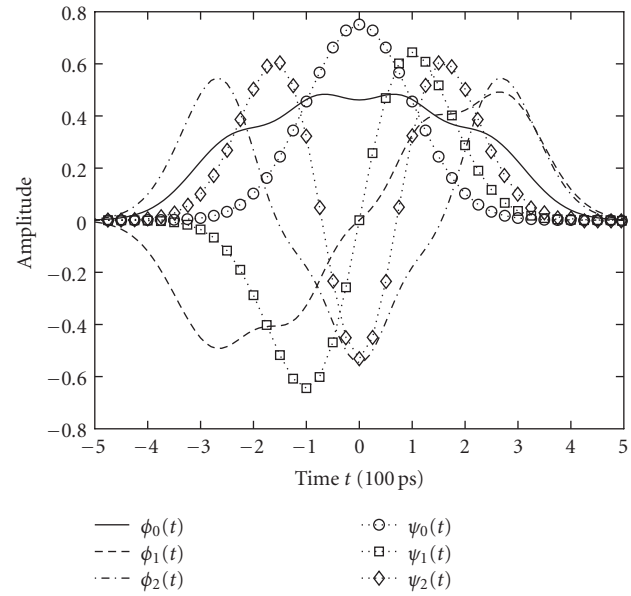

Figure 5: Comparison of a few jitter-robust waveforms $\phi_n(t)$ obtained with the proposed design against conventional Hermite pulses $\psi_n(t)$. Waveforms of orders 0, 1, and 2 are compared. All jitter-robust pulses were obtained with a Hermite space of dimension $N = 8$ and optimized to an RMS jitter of $\sigma_\tau = 100$ picoseconds.

Note that the effect of jitter shifts over $\phi_n(t)$ is merely to alter the output of the matched correlator, having little effect on its orthogonality towards the other waveforms $\phi_m(t)$. In addition, since $\vec{\chi}_n$ and $\psi_m(t)$ are orthonormal, all $\phi_n(t)$ have unitary energy, which means that the jitter-robust design inflicts no penalty in terms of power loss. Indeed,

$$\begin{aligned} \int_{-\infty}^{\infty} \phi_n(t)^2 dt &= \int_{-\infty}^{\infty} \left(\sum_{m=0}^{N-1} x_{m,n}\psi_m(t) \right)^2 dt \\ &= \sum_{m=0}^{N-1} (x_{m,n})^2 = 1. \end{aligned} \tag{39}$$

Finally, in the absence of jitter ($\tau = 0$), the matrix $\mathbf{A}(\tau)$ reduces to the identity matrix $\mathbf{I}$, $\rho_n = 1$, and $\phi_n(t) = \psi_n(t)$ for all n, which shows consistency in the design method.

4.2. Waveform examples

In Figure 5, a few waveforms obtained with the proposed method are compared against conventional Hermite pulses [1].

The jitter-robust waveforms $\phi_n(t)$ shown in Figure 5 were designed using a Hermite space of dimension $N = 8$ and optimized to stand an RMS jitter of $\sigma_\tau = 100$ picoseconds. Note that the shapes of $\phi_n(t)$ vary with these parameters.

It is seen from Figure 5 that the widths of the lower-order jitter-robust waveforms are only slightly larger than those of the corresponding conventional Hermites. In fact, all robust waveforms have widths closer to the highest-order Hermites of the Hermite space used in the design.

5. CORRELATION PROPERTIES OF PROPOSED WAVEFORMS

Equation (39) gives only the autocorrelation of the jitter-robust waveforms at $\tau = 0$. The general unified closed-form expression of the auto- and cross-correlation functions of these pulses can nevertheless be easily derived. By definition, and using (38), we have

$$R_{\phi_{m,n}}(\tau) \triangleq \int_{-\infty}^{\infty} \phi_m(t)\phi_n(t-\tau)dt = \int_{-\infty}^{\infty} \left(\sum_{i=0}^{N-1} x_{i,m}\psi_i(t)\right) \times \left(\sum_{j=0}^{N-1} x_{j,n}\psi_j(t-\tau)\right) dt. \tag{40}$$

Applying the Hermite decomposition (18) over $\psi_j(t-\tau)$, this simplifies to

$$R_{\phi_{m,n}}(\tau) = \sum_{i=0}^{N-1} \left(x_{i,m} \sum_{j=0}^{N-1} x_{j,n} c_{i,j}(\tau)\right). \tag{41}$$

Equation (41) can be put in the following matrix form:

$$R_{\phi_{m,n}}(\tau) = \vec{\chi}_m^{\mathrm{T}} \mathbf{A}(\tau) \vec{\chi}_n. \tag{42}$$

This is a closed-form expression since $\mathbf{A}(\tau)$ are completely and uniquely determined by the variable τ and its entries are given by (20).

Note that (42) can also be used to clearly demonstrate the robustness of the waveforms designed with the proposed design. Indeed, substituting (37a) into (42), we have

$$R_{\phi_{m,n}}(\tau) \approx \rho_n(\tau)\vec{\chi}_m \cdot \vec{\chi}_n = \rho_n(\tau)\delta_{n,m} \tag{43}$$

which signifies that, in the presence of a jitter shift τ, the correlator matched to the transmit (nth-order) waveform outputs $\rho_n(\tau)$, while all other correlators output zero.

Although a coherent jitter channel model was assumed in the design, (43) holds for the independent model with little modification (τ must be replaced by the N-tuple of independent jitter values $\vec{\tau}$). This is because the joint-diagonalization solution $\mathbf{X}$ also approximately diagonalizes the matrices of the form $\mathbf{A}(\vec{\tau})$, which is understood directly from the auto- and cross-correlations functions $R_{\phi_{n,n}}$ and $R_{\phi_{m,n}}$. Indeed, if $R_{\phi_{n,n}}$ and $R_{\phi_{m,n}}$ exhibit better properties than $R_{\psi_{n,n}}$ and $R_{\psi_{m,n}}$, random jitter shifts will affect a system using the pulses $\phi_n(t)$ less than one using $\phi_m(t)$.

Some of the autocorrelation functions of the conventional Hermites and the proposed jitter-robust pulses shown in Figure 5 are compared in Figure 6. It is observed that the autocorrelation functions of the proposed pulses exhibit significantly wider lobes in the vicinity of $\tau = 0$ than those observed with conventional Hermites.

Analogously, the cross-correlation functions of a few of the waveforms shown in Figure 5 are compared in Figures 7 and 8. It is observed that the cross-correlation values of the proposed waveforms are lower than those of the conventional Hermite pulses in the vicinity of $\tau = 0$.

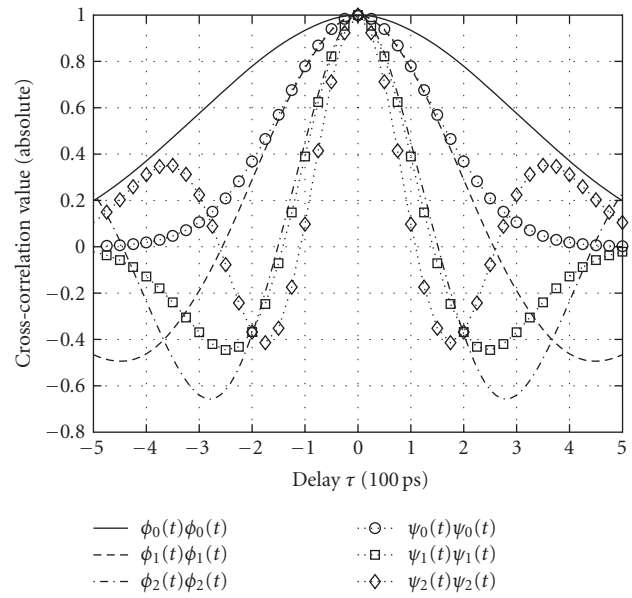

Figure 6: Comparison of the autocorrelation functions of a few jitter-robust waveforms $\phi_n(t)$ obtained with the proposed design against those of conventional Hermite pulses $\psi_n(t)$. Autocorrelations of the pulses of orders 0, 1, and 2 are compared. All jitter-robust pulses were obtained with a Hermite space of dimension $N = 8$ and optimized to an RMS jitter of $\sigma_\tau = 100$ picoseconds.

The efficacy of the jitter design, however, depends on the ratio between the standard deviation of the jitter process σ_τ and the pulse width T_p, as well as on the size N of the Hermite space used. For instance, a comparison of the cross-correlation functions of jitter-robust pulses obtained with Hermite spaces of sizes $N = 8$ and $N = 16$ is shown in Figure 9. It is seen that the design method yields better results when Hermite spaces of larger dimensions are used.

It must be noted, however, that although the jitter robustness of each waveform individually increases with the dimension of the Hermite space used in the design, the overall robustness of a system may reduce with its size, that is, the total number of jitter-robust orthogonal pulses used in the system. This is simply because in a larger system, a larger number of interfering components are added. Additional jitter robustness can, nevertheless, always be obtained by using in the design Hermite spaces of even larger dimensions, at the expense of an increased complexity.

Assume that a Hermite space of size N is used to design jitter-robust waveforms, but only a subset of the first $M \leq N$ of these waveforms is effectively used in the system. Although any subset of size $M \leq N$ could in principal be used, choosing the first M waveforms is optimal since the accuracy of the Hermite decomposition for lower-order pulses is better, as illustrated in Figures 2 and 3.

A good way to quantify the overall robustness of a given set of designed jitter-robust waveforms is to measure the distance of the Mth-order principal minors of the nearly diagonal matrices $\mathbf{D}(\tau) = \mathbf{X}^{\mathrm{T}}\mathbf{A}(\tau)\mathbf{X}$ to the M-by-M identity matrix.

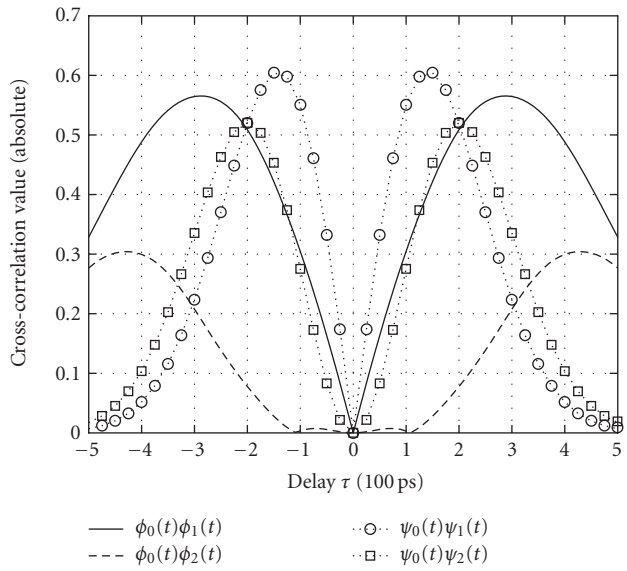

Figure 7: Comparison of the cross-correlation functions of a few jitter-robust waveforms $\phi_n(t)$ obtained with the proposed design against those of conventional Hermite pulses $\psi_n(t)$. Cross-correlations of the zeroth-order pulse with the first- and second-order pulses are compared. All jitter-robust pulses were obtained with a Hermite space of dimension $N = 8$ and optimized to an RMS jitter of $\sigma_\tau = 100$ picoseconds.

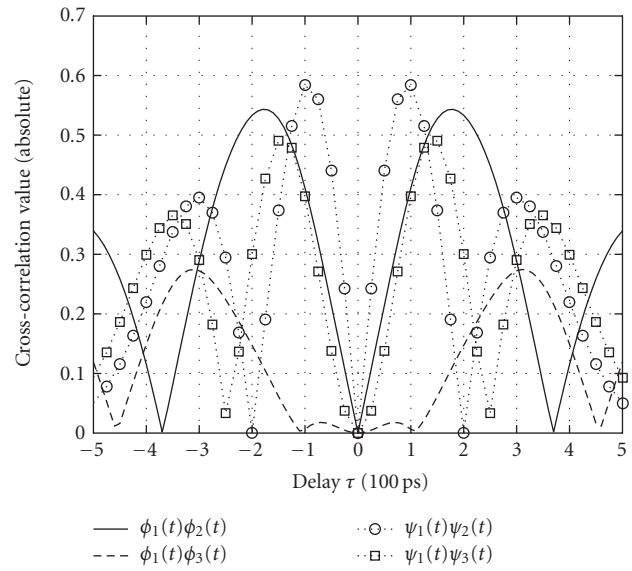

Figure 8: Comparison of the cross-correlation functions of a few jitter-robust waveforms $\phi_n(t)$ obtained with the proposed design against those of conventional Hermite pulses $\psi_n(t)$. Cross-correlations of the first-order pulse with the second- and third-order pulses are compared. All jitter-robust pulses were obtained with a Hermite space of dimension $N = 8$ and optimized to an RMS jitter of $\sigma_\tau = 100$ picoseconds.

This can be done with the following metric [21], which is hereafter referred to as the *jitter vulnerability coefficient*:

$$\zeta_{M,N}(\tau) \triangleq \left|\left|\mathbf{I} - \mathbf{D}_{M,N}(\tau)\right|\right|_F. \tag{44}$$

In the above, $\mathbf{D}_{M,N}(\tau)$ denotes the M-order principal minor of the N-by-N matrix $\mathbf{D}(\tau)$ and $\|\mathbf{B}\|_F$ denotes the Frobenius norm of $\mathbf{B}$, given by

$$\|\mathbf{B}\|_F = \sqrt{\text{trace}\left(\mathbf{B}^{\text{H}}\mathbf{B}\right)}. \tag{45}$$

At $\tau = 0$, we have $\mathbf{A} = \mathbf{I}$ and consequently, $\mathbf{D}(\tau) = \mathbf{I}$. Assuming that the pdf of τ is Gaussian, which decreases monotonically with the magnitude of τ, and given the criterion for choosing τ_k defined by (35), it is clear that $|\tau_k| - |\tau_{k-1}| < |\tau_{k+1}| - |\tau_k|$. In other words, the set of channel samples $\mathcal{A}_K$ is (intentionally) biased towards the more frequent lower values of τ. Consequently, we find that $\|\mathbf{I} - \mathbf{D}(\tau_k)\|_F < \|\mathbf{I} - \mathbf{D}(\tau_k + 1)\|_F$ for all k. This, again, indicates that the proposed pulses are strictly orthogonal at $\tau = 0$ and exhibit lower cross- and higher autocorrelations than conventional Hermites in that vicinity. This behavior is clearly observed in Figures 6 through 8.

Figure 10 shows a few plots of the jitter vulnerability coefficient $\zeta_{M,N}(\tau)$ against the magnitude of τ, for different combinations of M and N. The lower the value of $\zeta_{M,N}(\tau)$ is, the more robust the system is against jitter.

From the combined results of Figures 6 through 10, it is expected that a correlation-based UWB-IR system (including, but not limited to, PSM schemes) using the proposed waveforms exhibits a lower probability of error than one using conventional Hermites in the presence of jitter.

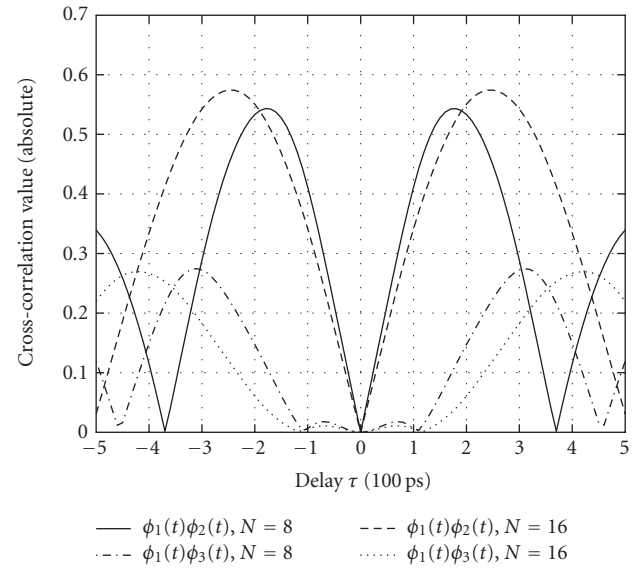

Figure 9: Comparison amongst the cross-correlation functions of a few jitter-robust waveforms $\phi_n(t)$ obtained with the proposed design. Cross-correlations of the first-order pulses with the second- and third-order pulses obtained with a Hermite space of dimension $N = 8$ are compared to those obtained with a Hermite space of dimension $N = 16$. All pulses were optimized to an RMS jitter of $\sigma_\tau = 100$ picoseconds.

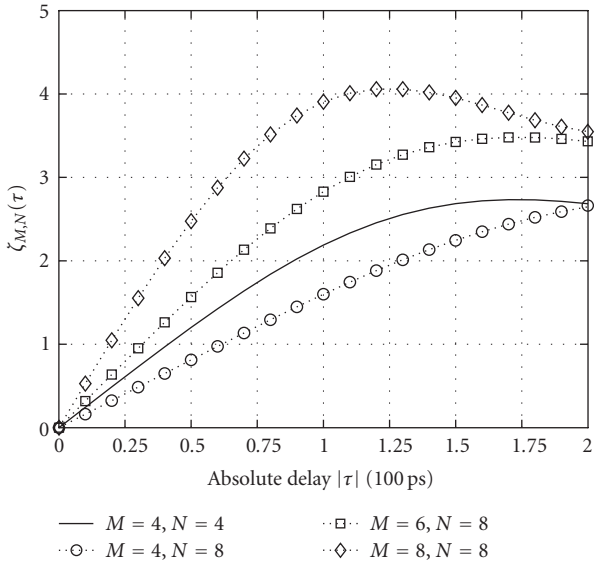

Figure 10: Jitter vulnerability coefficient against jitter magnitude. Curves for different combinations between the size of the Hermite space used in the design N and the number of orthogonal pulses used in the system M are shown. All results were obtained with waveforms optimized to an RMS jitter of $\sigma_\tau = 50$ picoseconds.

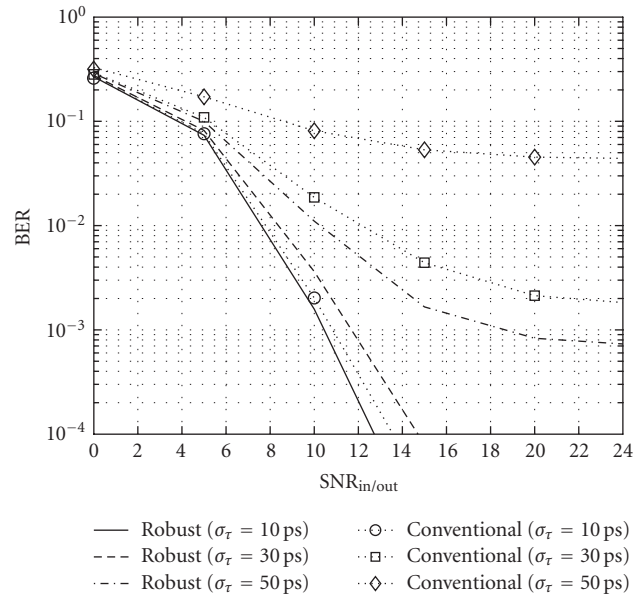

Figure 11: Comparison of BER performances of binary PSM-UWB-IR systems using jitter-robust waveforms obtained with the proposed design and using conventional Hermite pulses in coherent jitter channel with AWGN. All the jitter-robust waveforms used were designed with a Hermite space of size $N = 8$ and optimized to the respective RMS jitter of the channel. All binary PSM-UWB-IR systems use pulses of orders 0 and 1.

In the next section, simulation results are given which demonstrate the advantage of the proposed jitter-robust waveforms compared to the conventional Hermite pulses in a PSM-UWB-IR system as described in [23].

6. SIMULATIONS

Although UWB systems usually require several pulses per symbol transmission [2, 3, 15], our objective here is to demonstrate the performance gain achieved with jitter-robust pulse sets over systems using conventional Hermites. Consequently, in the following, only one-pulse-per-symbol PSM-UWB-IR systems in a single-user scenario are analyzed.

The signal-to-noise ratio ($\text{SNR}_{\text{in/out}}$) against which error rates are plotted is defined as the ratio between the power impinging onto the receive antenna (unitary) and the total noise at the output of the bank of correlators. This figure is used so that the loss incurred by splitting the incoming signal amongst N correlators is taken into account and is in accordance with the description of UWB-IR systems given in [15].

The bit error rate (BER) performances of PSM-UWB-IR systems using the proposed pulses are compared to those achieved using conventional Hermites in Figures 11 through 13.

First, in Figure 11, curves for a binary PSM scheme using zeroth-order and first-order pulses in noisy coherent jitter channels with RMS values of $\sigma_\tau = 10$, 30, and 50 picoseconds are shown. The jitter-robust waveforms were designed using a Hermite space of dimension $N = 8$.

The significant performance enhancement achieved with the jitter-robust waveforms is evident. While the conventional PSM-UWB-IR system [1] reaches a BER floor of about 2×10^{-3} errors/bit in a channel with RMS jitter of 30 picoseconds, in the same channel, the system using jitter-robust pulses do not show any error floor within the SNR span observed. Further, in a channel with an RMS jitter of 50 picoseconds, the PSM system with jitter-robust pulses exhibits a BER floor of 10^{-3} errors/bit, while the one using conventional Hermites is basically nonoperational.

It is important to emphasize that the above results were obtained at the ratio of 1 symbol/pulse, with pulses of 1 nanosecond of duration and without any error-correcting coding or transmit redundancy.

As discussed in Section 3.2, it is expected that the performance of jitter-robust pulses in an independent jitter channel is even better than that observed in a coherent jitter channel. This is demonstrated by the results shown in Figure 12. Comparing Figures 11 and 12, it is clear that the PSM scheme performs better in an independent jitter channel than in a coherent one. It is also learned from the comparison that while the PSM-UWB-IR system using conventional Hermites [1] is nonoperational in a channel with 50 picoseconds of RMS jitter (regardless of the independence of the jitter processes across correlators), the system using the proposed jitter-robust waveforms only looses about 2 dB at a BER of 10^{-4} errors/bit.

Finally, in Figure 13, the performances of jitter-robust and conventional M-ary PSM-UWB-IR systems in an

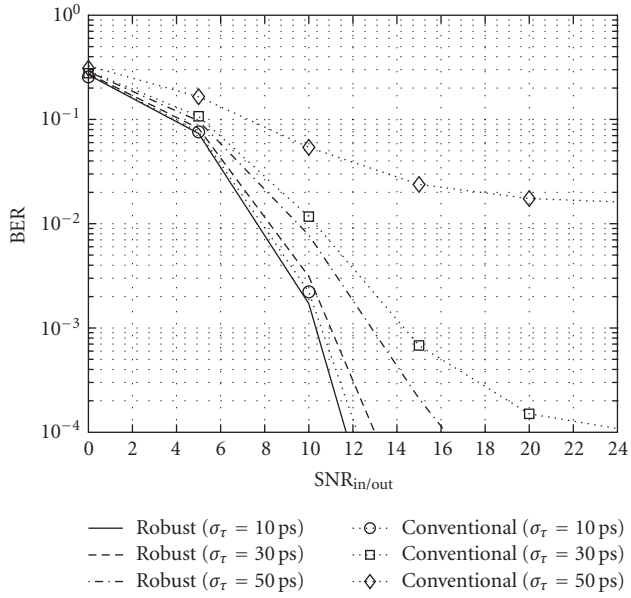

Figure 12: Comparison of BER performances of binary PSM-UWB-IR systems using jitter-robust waveforms obtained with the proposed design and using conventional Hermite pulses in independent jitter channel with AWGN. All the jitter-robust waveforms used were designed with a Hermite space of size $N = 8$ and optimized to the respective RMS jitter of the channel. All binary PSM-UWB-IR systems use pulses of orders 0 and 1.

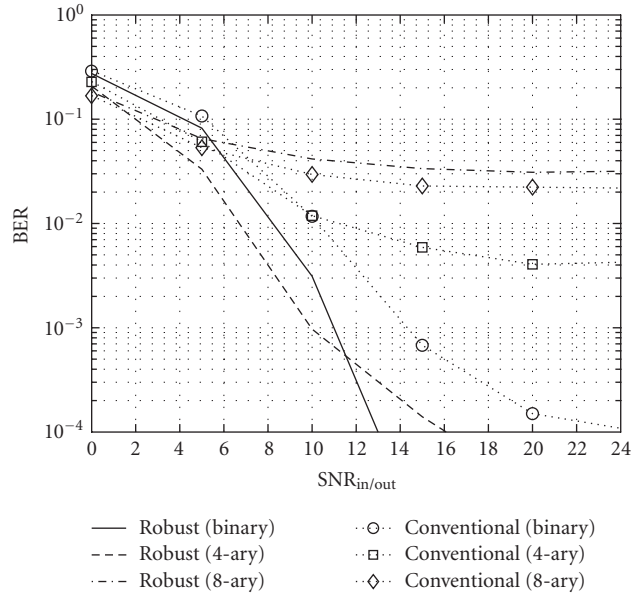

Figure 13: BER of M-ary PSM-UWB-IR that are proposed and conventional in noncoherent jitter channel with AWGN ($N = 8$; $\sigma_\tau = 30$ picoseconds).

independent jitter channel with 30 picoseconds of RMS are compared. Again, all jitter-robust waveforms were designed with a Hermite space of size $N = 8$ and optimized to stand the RMS jitter of the channel. As expected, it is seen that the gain achieved reduces if the size of the Hermite space used in the design is not sufficiently larger than the order of the modulation scheme employed.

It can also be seen that, in general, the performance of lower-order modulation schemes in low SNRs is worse than that of higher-order ones. This comes at no surprise given the $\text{SNR}_{\text{in/out}}$ figure used since, for a given $\text{SNR}_{\text{in/out}}$ value, the total noise at the output of the correlators is distributed over a lower number of filters.

7. CONCLUSIONS

The design of jitter-robust waveforms for UWB-IR communications was presented. The decomposition of jittered pulses onto finite Hermite spaces was used to establish a new multiplicative matrix-form jitter channel model, whose entries are given by the correlations between received pulses and their templates. The accuracy of the multiplicative model is directly proportional to the dimension of the Hermite space used and inversely proportion to the magnitude of jitter shifts.

A unified closed-form expression of the auto- and cross-correlation functions of Hermite pulses was provided, enabling the problem of jitter-robust waveforms to be transformed onto a generalized eigenproblem. The solution is given by a simplified version [22] of the numerically stable and robust Jacobi-like algorithm provided in [21], designed for simultaneous matrix diagonalization.

Examples of waveforms obtained with the design were compared to conventional Hermites. The unified closed-form expression of the auto- and cross-correlation functions of the jitter-robust waveforms was also provided and compared against those of conventional Hermite pulses.

As an application example, PSM-UWB-IR systems were considered. A brief analysis of these schemes in noisy jitter channels was also provided for the cases of fully independent and fully correlated (coherent) jitter processes observed across different correlators, which indicated the requirements for obtaining jitter-robust waveforms. Simulation results demonstrated the performance enhancement achieved using the proposed jitter-robust waveforms in noisy jitter channels with and without coherence in the pulse-shape domain.

In this work, we have focused on the problem of jitter and, for this reason, adhered to a channel model free of multipath. This decision was made deliberately, in order to isolate jitter as a major cause of degradation, allowing in-depth theoretical understanding of its effect on the properties of Hermite waveforms.

Despite simple, this assumption is (in addition to theoretically valuable) still representative of at least a few scenarios of practical interest. In the short run, for instance, one promising market for UWB devices is low data-rate communications with localization and tracking (LDR-TR) [24].

Restrictions on the transmit power (due to either regulations or target costs) limit the range of the UWB devices to a few tens of meters. Particularly in outdoor scenarios, where the likelihood of rich scattering is little, these low-power, range-limited devices experience a channel which approaches line-of-sight (LOS) or two-path models.

In the long run, on the other hand, it is fair to project that impulse-based UWB communications will achieve extremely high data rates, high enough to break beyond the competing multiband OFDM-based alternative (see the multiband OFDM alliance at http://www.multibandofdm.org) and through the limitations imposed by regulatory bodies, by using "signals with gigahertz bandwidths means that multipath is resolvable down to path differential delays and on the other of a nanosecond or less, that is, down to path length differentials on the order of a foot or less, [which] significantly reduces fading effects even in indoor environments,"—as put by Win and Scholtz in their classic paper [15].

Finally, we emphasize that ideas introduced here, and in our previous work [8], can in fact be used to design RAKE receivers with finger-wise adaptive templates that significantly improve performance under multipath conditions while avoiding massive equalization.

ACKNOWLEDGMENT

Part of this work appears in the Proceedings of the IEEE Global Conference on Communications 2003 (GLOBECOM '03).

REFERENCES

[1] M. Ghavami, L. B. Michael, S. Haruyama, and R. Kohno, "A novel UWB pulse shape modulation system," *Kluwer International Journal on Wireless Personal Communications*, vol. 23, no. 1, pp. 105–120, 2002.

[2] M. Z. Win and R. A. Scholtz, "Impulse radio: how it works," *IEEE Commun. Lett.*, vol. 2, no. 2, pp. 36–38, 1998.

[3] C. J. Mitchell, G. T. F. de Abreu, and R. Kohno, "Combined pulse shape and pulse position modulation for high data rate transmissions in UWB communications," *International Journal of Wireless Information Networks*, vol. 10, no. 4, pp. 167–178, 2003.

[4] S. Ciolino, M. Ghavami, and H. Aghvami, "UWB pulse shape modulation system using wavelet packets," in *Proc. IEEE International Workshop on Ultra Wideband Systems (IWUWBS '03)*, Oulu, Finland, June 2003.

[5] M. Pinchas and B. Z. Bobrovsky, "Orthogonal Laguerre polynomials pulses for ultra-wideband communication," in *Proc. IEEE International Workshop on Ultra Wideband Systems (IWUWBS '03)*, Oulu, Finland, June 2003.

[6] R. Dilmaghani, M. Ghavami, B. Allen, and H. Aghvami, "Novel UWB pulse shaping using prolate spheroidal wave functions," in *Proc. 14th IEEE International Symposium on Personal, Indoor and Mobile Radio Communications (PIMRC '03)*, pp. 602–606, Beijing, China, September 2003.

[7] J. A. N. da Silva and M. L. R. de Campos, "Orthogonal pulse shape modulation for impulse radio," in *Proc. IEEE International Telecommunications Symposium (ITS '02)*, pp. 916–921, Natal, Brazil, September 2002.

[8] G. T. F. de Abreu, G. J. Mitchell, and R. Kohno, "On the design of orthogonal pulse-shape modulation for UWB systems using Hermite pulses," *Journal of Communications and Networks*, vol. 5, no. 4, pp. 328–343, 2003, Special issue on ultra-wideband communications.

[9] A. D. Poularikas, *The Transforms and Applications Handbook*, CRC Press, Boca Raton, Fla, USA, 2nd edition, 2000.

[10] W. M. Lovelace and J. K. Townsend, "The effects of timing jitter and tracking on the performance of impulse radio," *IEEE J. Select. Areas Commun.*, vol. 20, no. 9, pp. 1646–1651, 2002.

[11] J. Romme and L. Piazzo, "On the power spectral density of time-hopping impulse radio," in *Proc. IEEE Conference on Ultra Wideband Systems and Technologies*, pp. 241–244, Baltimore, Md, USA, May 2002.

[12] D. Laney, G. M. Maggio, F. Lehmann, and L. Larson, "A pseudo-random time hopping scheme for UWB impulse radio exploiting bit-interleaved coded modulation," in *Proc. IEEE International Workshop on Ultra Wideband Systems (IWUWBS '03)*, Oulu, Finland, June 2003.

[13] S. Krishnan, O. Kyaw, V. Kumar, and P. Sharma, "The measured temporal and spectral characteristics of signals in a wireless UWB link," in *Proc. IEEE International Workshop on Ultra Wideband Systems (IWUWBS '03)*, Oulu, Finland, June 2003.

[14] S. Stroh, "Wideband: multimedia unplugged," *IEEE Spectr.*, vol. 40, no. 9, pp. 23–27, 2003.

[15] M. Z. Win and R. A. Scholtz, "Ultra-wide bandwidth time-hopping spread-spectrum impulse radio for wireless multiple-access communications," *IEEE Trans. Commun.*, vol. 48, no. 4, pp. 679–689, 2000.

[16] J. G. Proakis, *Digital Communications*, McGraw-Hill, New York, NY, USA, 4th edition, 2000.

[17] G. T. F. de Abreu, C. J. Mitchell, L. G. F. Trichard, and R. Kohno, "A note on the application of Hermite pulses in UWB communications," in *Proc. IEEE International Workshop on Ultra Wideband Systems (IWUWBS '03)*, Oulu, Finland, June 2003.

[18] A. Armogida, B. Allen, M. Ghavami, M. Porretta, G. Manara, and H. Aghvami, "Path-loss modelling in short range UWB transmissions," in *Proc. IEEE International Workshop on Ultra Wideband Systems (IWUWBS '03)*, Oulu, Finland, June 2003.

[19] T. P. Montoya and G. S. Smith, "A study of pulse radiation from several broad-band loaded monopoles," *IEEE Trans. Antennas Propagat.*, vol. 44, no. 8, pp. 1172–1182, 1996.

[20] J. R. Andrews, "UWB signal sources, antennas, and propagation," in *Proc. IEEE Topical Conference on Wireless Communication Technology (TCWC '03)*, Honolulu, Hawaii, USA, October 2003.

[21] A. Bunse-Gerstner, R. Byers, and V. Mehrmann, "Numerical methods for simultaneous diagonalization," *SIAM Journal on Matrix Analysis and Applications*, vol. 14, no. 4, pp. 927–949, 1993.

[22] J.-F. Cardoso and A. Souloumiac, "Jacobi angles for simultaneous diagonalization," *SIAM Journal on Matrix Analysis and Applications*, vol. 17, no. 1, pp. 161–164, 1996.

[23] L. B. Michael, M. Ghavami, and R. Kohno, "Multiple pulse generator for ultra-wideband communication using Hermite polynomial based orthogonal pulses," in *Proc. IEEE Conference on Ultra Wideband Systems and Technologies*, pp. 47–51, Baltimore, Md, USA, May 2002.

[24] I. Opperman, S. Zeisberg, F. Jondral, et al., "UWB low data rate communications with localization and tracking approach (LDR-LT), applications and challenges," in *Proc. 13th IST Mobile & Wireless Communications Summit*, Lyon, France, June 2004.

Giuseppe Thadeu Freitas de Abreu was born in Salvador, Bahia, Brazil, in December 1972. He received his B.E. degree in electronic engineering and a *Latus Sensu* degree of specialist in telecommunications from the Federal University of Bahia, Brazil, in 1996 and 1997, respectively. In 1997, he joined the Kohno Laboratory, Yokohama National University, Japan, as a research student and obtained his M.E. and Ph.D. degrees in electrical and computer engineering in March 2001 and 2004, respectively. In that period, he was awarded numerous prestigious scholarships from several institutions including the Ministry of Education, Culture, Sports, Science and Technology of Japan, the Rotary Yoneyama Memorial Foundation, the Yokohama Industrial Association, the Takaku International Scholarship Foundation, the Futaba Electric Memorial Foundation, and the Honjo International Scholarship Foundation. He was also the recipient of the Uenohara Foreign Student's Award from Tokyo University in 2000. Giuseppe Abreu has authored/coauthored 2 internationally registered patents (for Sony Corporation, Japan), several international journal papers, and various conference papers. His current research interests include smart antennas, beampattern synthesis, space-time signal processing and coding, MIMO systems, and ultra-wideband communications. He is currently a Research Scientist at the Centre for Wireless Communications, University of Oulu, Finland.

Craig John Mitchell was born in Johannesburg, South Africa, in November 1975. He received both his B.S. (*summa cum laude*) and M.S. degrees in electrical engineering from the University of the Witwatersrand, South Africa, in 1997 and 2001, respectively. He is currently working towards his Ph.D. at the Yokohama National University, Japan. His research interests lie in the areas of ultra-wideband systems and coding wireless communications.

Ryuji Kohno was born in Kyoto, Japan, in March 1956. He received his B.E. and M.E. degrees in computer engineering from Yokohama National University, in 1979 and 1981, respectively, and Ph.D. degree in electrical engineering from the University of Tokyo in 1984. He joined the Department of Electrical Engineering, Tokyo University, in 1984, and became an Associate Professor in 1986. From 1988 to 1997, he was an Associate Professor in the Division of Electrical and Computer Engineering, Yokohama National University, where he is now a Full Professor. He is the Chairman of the Societies of ITS and Software Radio of the IEICE, an Editor of the IEEE Transactions on Communications and on Information Theory and of the IEICE Transactions on Fundamentals of Electronics, Communications, and Computer Sciences. His research interests lie in several areas of wireless, optical and cable communications, coding and information theory, spread-spectrum and ultra-wideband systems, and so forth. He is a Member of IEEE, EURASIP, IEICE, IEE, and IPS of Japan and the author of several technical books and numerous papers.